REVIEW
doi.org/10.1002/elsa.202100163

Chemistry Europe
European Chemical Societies Publishing

Received: 23 September 2021
Revised: 27 December 2021
Accepted: 28 December 2021

Recent advances in ion-sensitive field-effect transistors for biosensing applications

Xiaohao Ma[1,2,†] | **Ruiheng Peng**[1,†] | **Wei Mao**[1,2] | **Yuanjing Lin**[1,2] | **Hao Yu**[1,2]

[1] School of Microelectronics, Southern University of Science and Technology, Shenzhen, China

[2] Engineering Research Center of Integrated Circuits for Next-Generation Communications, Ministry of Education, Southern University of Science and Technology, Shenzhen, China

Correspondence
Wei Mao, Yuanjing Lin, and Hao Yu, School of Microelectronics, Southern University of Science and Technology, Shenzhen 518055, China.
Email: maow@sustech.edu.cn, linyj2020@sustech.edu.cn, and yuh3@sustech.edu.cn

[†]These authors contributed equally to this work.

Funding information
Engineering Research Center of Integrated Circuits for Next-Generation Communications, Grant/Award Number: Y01796303; Southern University of Science and Technology, Grant/Award Numbers: Y01796108, Y01796208; Shenzhen Science and Technology Program, Grant/Award Number: KQTD20200820113051096; National Key R&D Program of the Ministry of Science and Technology, Grant/Award Number: 2021YFE0204000; National Natural Science Foundation of China (NSFC) Key Program, Grant/Award Number: 62034007; Shenzhen Nanshan Bureau of Science and Technology, Grant/Award Numbers: K21799122, K21799109

Abstract

Over the past decades, considerable development and improvement can be observed in the area of the ion-sensitive field-effect transistor (ISFET) for biosensing applications. The mature semiconductor industry provides a solid foundation for the commercialization of the ISFET-based sensors and extensive research has been conducted to improve the performance of ISFET, with a special research focus on the materials, device structures, and readout topologies. In this review, the basic theories and mechanisms of ISFET are first introduced. Research on ISFET gate materials is reviewed, followed by a summary of typical gate structures and signal readout methods for the ISFET sensing system. After that, a variety of biosensing applications including ions, deoxyribonucleic acid, proteins, and microbes are presented. Finally, the prospects and challenges of the ISFET-based biosensors are discussed.

KEYWORDS
biosensing applications, gate materials, gate structures, ISFETs

1 | INTRODUCTION

Over years of study, silicon-based biosensors have been employed in various bioanalytical fields due to their favorable characteristics, such as high sensitivity, integration capability, miniaturized device volumes, and relatively low cost. Impressive progress has been achieved in developing silicon-based biosensors based on a variety of mechanisms, such as optical waveguide biosensors, high electron mobility transistors, micro-electromechanical

REVIEW
doi.org/10.1002/elsa.202100163
Chemistry Europe
European Chemical Societies Publishing

systems sensors, and ion-sensitive field-effect transistors (ISFETs).[1–4] Among them, the ISFET was one of the first miniaturized devices as a silicon-based chemical sensor. The first ISFET was proposed with Na^+ sensitivity by Bergveld in 1970.[5] In an ISFET, the obtained source-drain current shows a linear relationship with the correlative ion concentration. Such a concept demonstration stimulates research efforts in further modification of traditional transistors to obtain superior biosensing characteristics.

Research advances in material engineering and device structural design have largely widened the applications of ISFETS in clinical monitoring, personalized healthcare, disease control, and so forth.[6,7] A variety of sensitive layers in ISFETs were proved to have desirable sensitivity for ion detection such as potassium ion (K^+), sodium ion (Na^+), cobalt ion (Co^{2+}), aluminum ion (Al^{3+}), and ammonium ion (NH_4^+).[5,8–12] In 2011, Rothberg et al. demonstrated the deoxyribonucleic acid (DNA) sequencing method using the ISFET, which further broadened the application scenarios of transistor-based sensors for sensing biomacromolecules.[13] Moreover, ISFET-based wearable sensing systems, including human sweat and plasma monitoring, were designed for in vivo and in vitro healthcare.[14–18] Specific detections of other macromolecules such as proteins, antigens, and enzymes, were also realized.[19–21] Apart from research efforts on sensitive layer engineering, device structural designs and gate materials have been extensively studied. Bausells et al. further modified the gate structure of the ISFET to ensure its compatibility with the standard complementary metal-oxide-semiconductor (CMOS) process.[22] Different channel materials like graphene and molybdic sulfide (MoS_2) were also reported to enhance sensing performance.[23,24] Moreover, system topologies were studied to realize the super-Nernstian ion-sensing sensitivity.[25,26]

This paper reviews the advanced ISFETs for biosensing applications with discussion on the recent reports on the materials, structures, and topologies from component to system. We presented the system-level design of integrated ISFET-based biosensors, including the readout circuit and integrated systems. The fundamentals and mechanisms of the ISFET will be briefly introduced in Section 2 and a summary of recent advances in gate materials will follow in Section 3. Representative reports on gate structures will then be summarized in Section 4 and the signal readout topologies will be reviewed in Section 5. Additionally, research on biosensing applications of ISFET will be summarized based on different gate materials in Section 6. Section 7 will include a discussion on the challenges and future perspectives in the field of ISFET-based bioelectronics.

2 | FUNDAMENTALS AND MECHANISMS

Research efforts have been devoted to continuously optimizing the performance of the ISFET towards low cost, high sensitivity, high stability, and good integration. Figure 1a,b shows the classic schematics of the traditional metal-oxide-semiconductor field-effect transistor (MOSFET) and ISFET. MOSFET is a type of insulated-gate field-effect transistor and its voltage of the covered gate determines the electrical conductivity of the device; this ability to change conductivity with the amount of applied voltage can be used for amplifying or switching electronic signals. Compared to the commonly seen MOSFETs, the metal gate is removed and a reference electrode is included to provide biased voltage in an ISFET. The reference electrode and silicon dioxide (SiO_2) insulation layer are immersed in the target solution. A sensitive layer will be further prepared on the insulation layer, such as tantalic oxide (Ta_2O_5), aluminum oxide (Al_2O_3), and silicon nitride (Si_3N_4). During the measurement, a certain voltage V_{GS} is applied to the reference electrode, and V_{DS} is applied between the drain and source of the ISFET. Thus, a dynamic source-drain current is obtained when solution pH changes. The site-binding model proposed by Yates et al. in 1974,[27] which figures out the formation of ion pairs at the oxide/aqueous electrolyte interface, is well-known in explaining the mechanism of ISFET in ion sensing. Besides, according to the Gouy-Chapman theory, an electric double layer is formed at the interface between solution and sensing layer, and ions in the solution can combine with functionalities at the surface, which then changes the surface potential of the sensing layer.[28,29] As for the ISFET-based pH sensor, which employs the SiO_2 as an insulation layer, reactions that happened at the interface include[30]:

$$\mathrm{SiOH} \leftrightarrow \mathrm{SiO^-} + \mathrm{H^+} \tag{1}$$

$$\mathrm{SiOH} + \mathrm{H^+} \leftrightarrow \mathrm{SiOH_2^+} \tag{2}$$

in which the hydroxyl groups donate or accept protons. The surface potential of the insulator is further altered, resulting in the change of the threshold voltage V_{th} (the gate-source voltage is needed when the inversion layer is formed in FET) of the ISFET. Figure 1c shows a simple circuit diagram of an ISFET sensing system.

Figure 1d shows a capacitance model of the ISFET in the unmodified CMOS process, which is fabricated with standard CMOS technologies and can be used for pH sensing without further modification.[31] When a sensing layer comes into contact with the solution, the transfer of electrons/ions between the two phases creates an excess charge

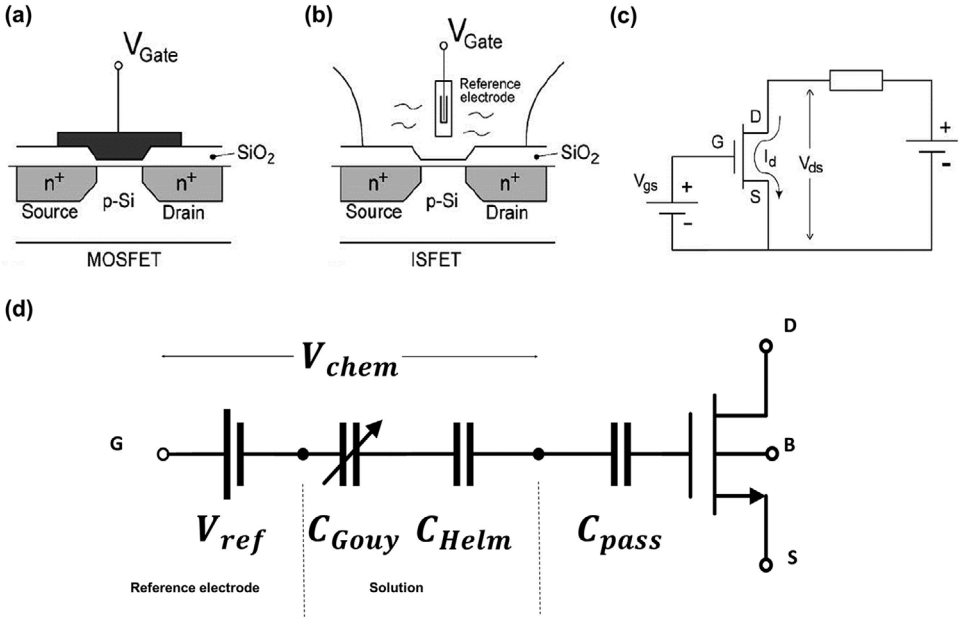

FIGURE 1 Typical device structures of (a) metal-oxide-semiconductor field-effect transistor (MOSFET) and (b) Ion-sensitive field-effect transistor (ISFET). (c) Simple circuit diagram of an ISFET sensing system. (d) Capacitance model of an ISFET in unmodified complementary metal-oxide-semiconductor (CMOS) process[31]

in each phase, known as the Helmholtz layer. Based on the electrical double-layer theory, the C_{Gouy} and C_{Helm} refer to the capacitances of the Gouy-Chapman layer and the capacitances of the Helmholtz layer, respectively; the C_{pass} stands for the capacitance of the passivation layer above the insulator. And the surface potential at the passivation layer V'_G depends on the pH of the solution[32]:

$$V'_G = V_G - V_{chem} = V_G - (\gamma + \alpha S_N pH) \quad (3)$$

where γ is a constant, S_N is the ideal pH sensitivity, and α is the sensitivity deviation. The threshold voltage of the device can be further expressed as:

$$V_{th} = V_{th(MOSFET)} + \gamma + \alpha S_N pH \quad (4)$$

From the circuit shown in Figure 1c, when the FET works in the saturation region, the drain-source current can be calculated as:

$$I_{DS} = \mu C_{OX} \frac{W}{L}[(V_{GS} - V_{th}) V_{DS} - \frac{1}{2} V_{DS}^2 \quad (5)$$

where μ is the carrier mobility, and C_{OX} refers to the capacitance of the oxide layer, W/L is the aspect ratio of the FET channel, where W and L refer to the width and length of the channel, respectively, and V_{DS} remains constant. Therefore, a different pH environment leads to different threshold voltages. By measuring the changes in V_{th} or I_{DS}, changes in pH can be determined.

Table 1 summarizes some ISFET devices based on different sensitive layers, channel materials, and ideal biomarkers with specific resolution, which will be discussed thoroughly in the following section. In general, the fabrication of the device mainly relies on CMOS processes, including materials deposition, coating, photolithography and etching to achieve particular electrode patterns. Various deposition methods have been widely adopted for gate materials fabrication. For instance, oxide membranes are extensively deposited by chemical vapor deposition, physical vapor deposition, atomic layer deposition (ALD), and so forth.[14,24,33] Other materials such as graphene channels can be deposited by thermal evaporation, spin-coating, and E-beam evaporator.[17,34,35]

3 | GATE MATERIALS

Typically, ISFET gate materials refer to a sensitive layer in direct contact with the targeted solution, and this layer is known as a gate dielectric/insulator. ISFETs are one of the successions of MOSFETs to achieve CMOS-based chemical sensing; thus the flow of source-drain current is controlled by the gate potential generated at the interface between the sensitive membrane and the solution. Stable sensing signals can be extracted when the ISFET is coupled with a reference electrode, such as silver/silver chloride (Ag/AgCl) electrode.[45] For a traditional pH-sensing ISFET, its threshold voltage depends on the pH of the targeted solutions in contact with its ion-sensitive

TABLE 1 Summary of the ion-sensitive field-effect transistor (ISFET) materials and sensing systems

Sensitive layer	Channel material	Preparation Process	Monitoring Target	Sensitivity/ Resolution	Ref.
Nanocrystalline Graphene	Graphene	Thermal evaporation, photolithography	pH	140 mV/pH	[34]
Ionophore membranes	Graphene	CVD, thermal evaporation	K^+, Na^+, NH_4^+	6.27, 17.4 and 2.9 μA/decade	[9]
L-phenylalanine membrane	Graphene	CVD, thermal evaporation	Na^+, Co^{2+}, Al^{3+}, Cu^{2+}	0. 17 pmol/L for Cu^{2+}	[33]
K^+ ionophore membrane	Graphene	Cold walled CVD, thermal evaporation	K^+	39 ng/L	[8]
Al_2O_3	MoS_2	Atomic layer deposition (ALD), low-power oxygen plasma	pH	>50 mV/pH	[36]
Al_2O_3/ hafnium oxide (HfO_2)	MoS_2	Mechanical exfoliation, E-beam evaporation, ALD	pH	~58.7 mV/pH	[24]
Glucose oxidase	MoS_2	E-beam evaporation, micromechanical exfoliation	Glucose	260 mA/mM	[37]
DNA-Au NPs hybrid structure.	MoS_2	Sputter, lithium ion exfoliation method	Hg^{2+}	1 pM to 100 nM	[38]
Al_2O_3	Black Phosphorus (BP)	E-beam evaporation, ALD	Immunoglobulin G.	~10 ng/ml	[39]
dithiothreitol (DTT)/Au NPs	Black Phosphorus (BP)	Laser direct writing, sputter	As^{3+}	1 nM to 1000 nM	[40]
(3-aminopropyl) triethoxysilane (APTES)	MXene/graphene	E-beam evaporation, CVD	2019-nCoV spike protein	1 fg/ml to 10 pg/ml	[41]
$Ti_3C_2T_x$ MXene	Si	Photolithography, etching	Ag^+	0.5μM to 10μM	[42]
Ta_2O_5	Si	1.2μm-CMOS, physical vapor deposition (PVD), etching	L-carnitine	18.0 $\pm$ 1.7 mV/μM	[21]
Al_2O_3	Si	E-beam evaporation, liftoff, etching	Sweat pH	51.2 mV/pH	[14]
Indium oxide	Indium phosphide (InP)	Molecular-beam epitaxy evaporation, liftoff, photolithography, inductively coupled plasma (ICP)	pH	58.3 mV/pH	[35]
Al_2O_3	Si-Nanowire (SiNW)	Photolithography, thermal oxidation, ALD	pH	48 mV/pH	[43]
Polyethylene glycol (PEG)	Si-Nanoribbon	Photolithography, etching, E-beam evaporation	Prostate specific antigen	100 pM to 100 nM	[17]
Gold (Au)	SiNW	ALD	Na^+	44 mV/decade	[44]

Abbreviations: CVD,chemical vapor deposition; PVD, physical vapor deposition.

barrier as shown in Figure 1b. For inorganic ions sensing, different sensitive membranes are deposited on the gate layer. For detection of other macromolecules, a certain amount of enzyme/antibody/RNA could be added for a specific reaction. The change of protons in the solution during the reaction indicates the different concentrations of the analytes being tested.

According to the Nernst equation, the magnitude of total potential E is related to the ion concentration. For a complete electrochemical reaction (full cell), the equation can be written as follows:

$$E = E_0 + \frac{RT}{nF}\ln\frac{C_{ox}}{C_{red}} \quad (6)$$

where E_0 is the standard cell potential, $\frac{RT}{F}$ is a constant, n is the number of electrons transferred in the cell reaction, and $\frac{C_{ox}}{C_{red}}$ is the ratio of oxidant concentration to reductant concentration. For pH sensing, $(E - E_0)$ delivers a linear correlation of 0.0592 V/decade with proton (H^+) concentrations. Therefore, the gate potential is adjusted by ion concentration, which then leads to the change of current response.

Since the metal gate in a traditional MOSFET was first replaced by the aqueous solution to form an ISFET, a variety of materials have appeared in the history of ISFETs.[46] Oxides play an important role and form the foundation of the ISFET gates.[20,47–49] The basic principle is that the H^+ released from the dynamic solution will affect the pH in the well. This induces a change in the surface potential of the oxide layer as well as the potential between the gate and base of the underlying field effect. Apart from oxides, many composite materials with modified morphologies and properties can also be utilized as ion-selective membranes. In this part, gate materials including thin-film sensitive layers, two-dimensional (2D) materials, and a wide range of nanostructured functionalized materials will be summarized in accordance with the development of ISFETs.

3.1 | Sensitive thin films

SiO_2: SiO_2 is one of the materials that has been widely employed for the ISFET gate fabrication. The performance of single-layered SiO_2 has been further improved by stacking with other thin films, such as $SiO_2/HfO_2/Al_2O_3$.[50] Lee et al. first applied $Al/SiO_2/Si$ layers as a sensor for antigen test of hepatitis B (HBsAg) in order to avoid the time-consuming steps and low sensitivity in high ion concentration.[20] The HBsAgs hold strong negative charges and the positive hydrogen ions in the solution cluster near the functional groups causing pH change of the sensing oxide.

Ta_2O_5: The first Ta_2O_5 gate ISFET was fabricated in 1981 by Matsuo et al., and Ta_2O_5 was one of the most suitable materials known for that time as the gate layer for pH-sensing.[51] Before long, the first Ta_2O_5 gate ISFET with differential amplifier was fabricated in 1989 by Wong et al. The output of an amplifier with a Ta_2O_5/SiO_2 gate ISFET (58–59 mV/pH) was differentially amplified against the output of another amplifier with a $SiO_xN_y/Si_3N_4/SiO_2$ gate ISFET (18–20 mV/pH).[52] In this system, an external reference electrode was not required because of its unique topology. Until now, Ta_2O_5 involves various biosensing fields, including enzyme detecting, live-cell monitoring, and even gas sensing.[16,21,53]

Al_2O_3: Al_2O_3 as a chemically stable material has been widely utilized in pH sensing with satisfactory performance since 1979.[54] As shown in Figure 2a, an ISFET for pH sensing is reported by Choi and co-workers.[55] When the ISFET was in solution, the Al_2O_3 film surface charged with the proton concentrations, which alters the surface potential and the source-drain current as well. For small sensing areas (~0.1 mm^2), the pH sensitivity of a commercial FET is reduced dramatically. While in the case of this Al_2O_3 ISFET, the pH sensitivity is unaffected for smaller sensing areas and makes it possible for the analysis of integrated samples. Recently, other Al-based materials are also adopted as the ISFET's gate, such as aluminum nitride and metallic aluminum.[56,57]

Nitrides: Nitrides enable a broad range of biomarkers sensing. For instance, Si_3N_4 performs superior water tightness and chemical stability for H^+ sensing. With an ion-sensitive layer on top of the Si_3N_4 gate, the device can then be utilized for a variety of biomarkers sensing.[54] Moser et al. demonstrated a CMOS platform with Si_3N_4 layer for on-chip real-time amplification and DNA detection, which emerges from the pH sensing prototype, as shown in Figure 2b. Its output signals show a linear spread of 0.3% with a high pH sensitivity of 3.2 μs/pH.[58] Moreover, Toumazou et al. detected the nucleic acid polymerization reaction by using Si_3N_4 as gate layer.[59] Indium nitride (InN) is another promising material for obtaining high sensitivity of pH sensing. As shown in Figure 2c, an ultrathin InN ISFET is prepared and shows a sensitivity of 58.3 mV/pH in the range of 2–12 pH, with a resolution down to less than 0.03 pH and a response time fewer than 10 s.[35] The strong accumulation of surface electrons in InN leads to a huge ion-induced surface potential for current transconductance in the ultra-thin conductive channel. Consequently, adequate gate bias in the electrolyte can effectively modulate the electron density in the ultra-thin conductive channel and significantly increase the current variation ratio. Gallium nitride (GaN) with a wide energy gap can be engineered through heterostructure design. It has a high transconductance at around zero gate-drain voltage and thus enables a high sensitivity.[11] Matthew et al. demonstrated that a GaN ISFET coated with an ion-selective membrane to detect nitrate ions in solution and observed a linear response range of 10^{-6}–10^{-3} M.

Other oxides: In recent years, zinc oxide (ZnO), palladium oxide (PdO), HfO_2, and many composite oxides have been adopted as ion-sensitive membranes with attractive properties.[26,36,60–62] For instance, ZnO can obtain a wide range of pH sensing with linear response, and the HfO_2 gate deposited by ALD can minimize the oxygen vacancies to reduce the attached ions on the surface of the sensing film. One of the most eye-catching progress was that Nakata et al. used an indium-gallium-zinc-oxide thin film

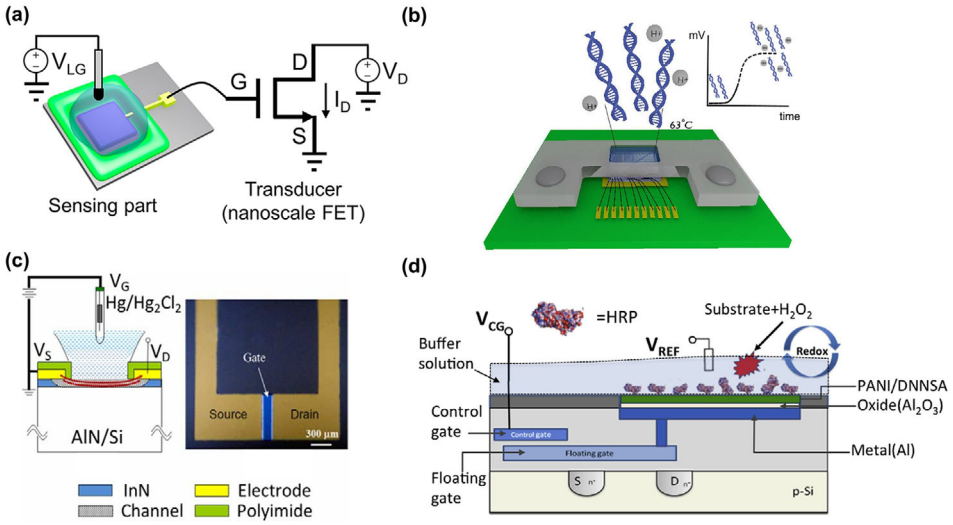

FIGURE 2 Ion-sensitive field-effect transistors (ISFETs) with different sensitive thin-film materials. (a) The nanoscale FET-based extended-gate biosensor with an $A1_2O_3$ layer.[55] (b) The complementary metal-oxide-semiconductor (CMOS) platform is used for real-time detection of deoxyribonucleic acid (DNA) with the Si_3N_4 layer.[58] (c) Schematic of a 10-nm-thick InN ISFET.[35] (d) Cross-sectional view of an ISFET modified with PANI/DNNSA layer for H_2O_2 sensing[65]

for the n-type gate material and the pH-sensing membrane simultaneously.[14] In this work, a flexible sensor based on the as-prepared oxide film was integrated with a temperature sensor for real-time measurements. It paved the way for fully integrated and flexible personalized bioelectronics in the future. In addition, Singh and coworkers first demonstrated indium-zinc oxide ($InZn_xO_y$) could be applied for pH sensing.[63] It delivered a low drift rate of 2.08 mV/h and a stable performance after 500 bending cycles with a homogeneous and dense $InZn_xO_y$ thin film.

Polymers: As summarized above, inorganic materials have been widely utilized for gate fabrication to obtain desirable pH sensing. Apart from these, polymer/organic gates expand the types of targeted analytes and pave the way for multiple analytes detection with ISFETs. For instance, Zhang et al. modified the polyaniline protonated with dinonylnaphthalene sulfonic acid (PANI/DNNSA) as gate material for an ISFET polyethyleneimine (PEI) sensor.[64] PEI serves as a proton sponge and absorbs protons from the PANI backbone. The released protons cause a nearby pH decrement, inducing an ISFET output signal between the source and drain electrodes. It was also found that the PANI/DNNSA layer largely improved the device stability under 100% relative humidity (RH). The application of the PANI/DNNSA membrane was further explored by the same research group.[65] Figure 2d illustrates its working principle as a sensing gate for hydrogen peroxide (H_2O_2) detection in horseradish peroxidase (HRP) catalyzed redox reaction. Once HRP is immobilized on the PANI/DNNSA functionalized sensing surface, hydrogen peroxide (H_2O_2) is reduced into water. The detection of enzyme-catalyzed reactions on an ISFET device opens possibilities for ultrasensitive enzyme-sensing on a CMOS bioelectronic platform. Other organic materials such as hydrogel, polystyrene, and polyvinyl chloride can be deposited for specific biosensing applications.[66–68]

3.2 | 2D materials

Graphene: Graphene has higher carrier mobility than silicon at room temperature, which indicates that the electron mobility remains more stable with temperature change.[69] Owing to its extreme sensitivity to surface charge and strong interaction with ionic adsorbates, it can serve as an excellent material for an electron-proton transducer. A large library of ISFETs employing various graphene-based functionalized layers has been demonstrated so far. For instance, Li et al. reported graphene-based ISFETs for K^+ detection via a valinomycin-based ion-selective membrane.[10] The sensitivity is 61 ± 4.6 mV/decade with a wide sensing range of 1μM–20 mM, which is superior to commercial Si-based ISFETs. Another ISFET device with L-phenylalanine's structure for sensing different metal ions was proposed by Alves et al.[33] As shown in Figure 3a, L-phenylalanine's aromatic group allows a π–π interaction with graphene, and the carboxylic acids and amino groups can coordinate with metal ions. Hence, one end of the L-phenylalanine attaches to the graphene, and the other end binds to the targeted ions. From the comparison of pristine and functionalized graphene, it is recognized that functionalized graphene improves the accuracy

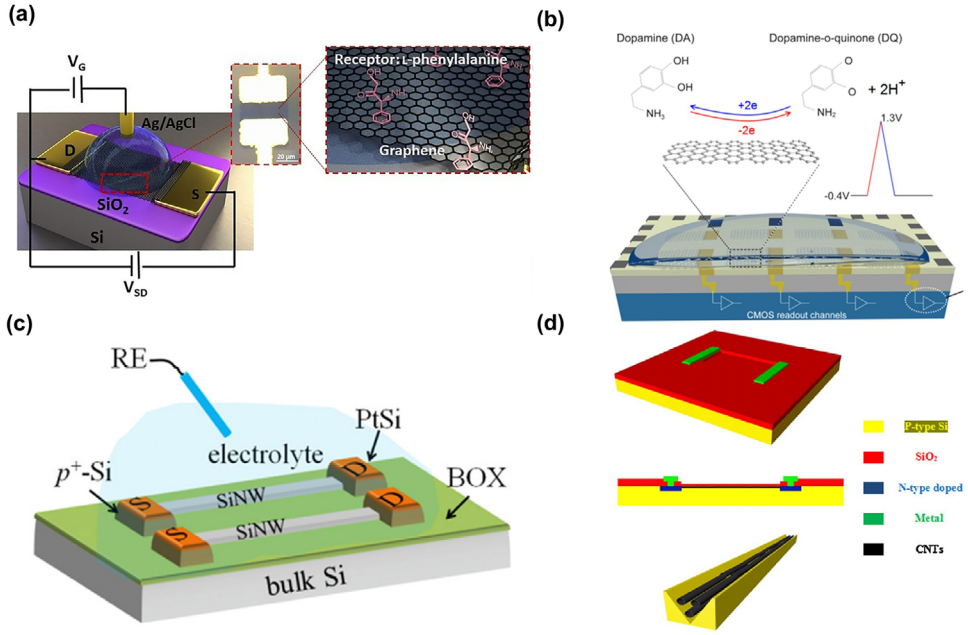

FIGURE 3 Ion-sensitive field-effect transistors (ISFETs) with 2D and a variety of nanostructured materials. (a) ISFET device based on graphene with the L-phenylalanine receptor.[33] (b) Complementary metal-oxide-semiconductor (CMOS)-graphene sensor arrays for multi-points DA molecules sensing.[70] (c) Three-dimensional sketch of silicon nanowire (SiNW)-ISFETs.[84] (d) The structure design of the carbon nanotube (CNT)-ISFET pH sensing device[85]

for ion detection and enables stable multi-ion detection, including Na^+, Co^{2+}, and Al^{3+}. Ibrahim et al. applied the Nikolskii-Eisenman equation as an extension to the Nernst equation to include the potential contribution from multiple ion species[9]:

$$E_i = E_o + \alpha ln10\frac{RT}{zF}\log(a_i + \sum_{j\neq i}^{n} k_{ij}a_j^{\frac{z_i}{z_j}}) \quad (7)$$

where the ion activity is a_i (the charge is now z_i) for a specific analyte. The interfering ion is marked as j with corresponding activity a_j and charge z_j, $\alpha ln10\frac{RT}{zF}$ is a constant for a certain kind of ion, and $(E_i - E_0)$ is the potential difference. k_{ij} is the selectivity coefficient and the smaller the k_{ij} values, the less impact the interfering ion will have on the measured potential. ISFET arrays were designed for real-time concentration measurements of K^+, Na^+, NH_4^+, nitrate ion (NO_3^-), sulfate ion (SO_4^{2-}), and chloride ion (Cl^-) simultaneously. By applying Nikolskii-Eisenman analysis, selective ion sensing was demonstrated. Apart from metal ions, high-density measurements of dopamine (DA) can also be realized with a heterogeneous CMOS-graphene sensor array.[70] Figure 3b shows that extra electrons are generated due to the redox reaction of DA molecules with carbon atoms on graphene. The high resolution of sensor pixels creates an opportunity for accurate and multi-point in vivo measurements. In addition, a graphene-based ISFET was reported to have a pH sensitivity beyond the Nernst limit[34]. Defect-engineered graphene was designed as an ISFET sensing channel, leveraging charge transfer effect, and achieved a beyond-Nernstian pH response (~140 mV/pH) with nanocrystalline graphene.

Black phosphorus: As a layered semiconductor with a controllable bandgap and high carrier mobility, black phosphorus (BP) is one of the most promising materials for nanoscale transistors. In recent years, it has been adopted for the detection of heavy metal ions, nitrogen dioxide gas, and immune protein.[39,71,72] For example, Zhou et al. utilized BP membrane as a conductive channel to uniformly disperse Au nanoparticles (NPs) and realized Arsenic ion (As^{3+}) detection from 1 to 1000 nM. The reported BP/Au NPs/dithiothreitol hybrid structure has a simple manufacturing process and excellent sensing performance, which is prospective for real-time ion detection.

Molybdenum sulfide: In 2011, Kis and co-workers made the first transistor with a single sheet of molybdenum sulfide (MoS_2, down to 0.65 nanometers thick).[73] Note that, 2D MoS_2 has then attracted tremendous research interest due to its unique structure and semiconductor property. For instance, Wang et al. reported a highly stable and repeatable MoS_2 FET biosensor with $Al_2O_3/HfO_2/MoS_2/SiO_2$ hybrid structure[74]. Compared with the HfO_2-gated sensor, this sensor has higher current sensitivity (~105-fold) and a relatively small limit of

detection (LOD) of 0.01 pH. Moreover, Wei et al. improved the multilayer gate structure to achieve a low LOD of 1.54×10^{-3} pH and reduced the drift value to 4 mV/h. In addition, MoS_2-gated ISFET has been reported for heavy metal ions, glucose, hydrogen peroxide, and proteins sensing.[37,38,75,76]

2D transition metal carbides, carbonitrides, and nitrides: 2D transition metal carbides, carbonitrides, and nitrides (Mxenes) are novel 2D materials with graphene-like structures, consisting of transition metal carbides, nitrides, or carbonitrides. Its superior conductivity allows ions to move with much less resistance and thus has been applied to biosensors since 2011.[77] For instance, ISFETs based on $Ti_3C_2T_x$ have been reported for ion sensing, including mercury ion, silver ion, alkaline ion, and so forth.[42,78,79] Xu et al. further designed an ultrathin (~5 nm) MXene-micropattern-based FET for DA detection, showing a detection range from 100 nM to 50 μM.[80] During the COVID-19 pandemic, Li et al. also invented a FET sensor based on Mxene-graphene, which can detect the virus in a low-cost, ultra-sensitive, fast, and specific way.[41] Based on the antibody-antigen sensing mechanism, the MXene-graphene FET sensor shows a low LOD (1fg/ml for recombinant 2019-nCoV spike protein) and fast response time (50 ms).

3.3 | Other nanostructured materials

Si nanowires: ISFETs based on Si-nanowire (SiNW) have a high surface-to-volume ratio in the nanowire-type channel. It increases the threshold voltage and gate capacitance, and thus proceeds excellent ion sensing properties. For example, via traditional silicon top-down techniques, Kim et al. fabricated an ISFET with SiNW in a width of 50 nm wide and length of 10 μm.[81] The ISFET delivered a sensitivity of 40 mV/pH, and the signal-to-noise ratio of the device is estimated at a resolution of 0.016 pH from the measured noise results. Other ISFETs based on Si nanowires, such as dual-gate FETs, dual-mode amplification FETs, and stacked SiNW FETs are also presented for pH sensing in recent years.[12,82,83] In addition, various ion sensing can be achieved by using self-assembled monolayers (SAM). Wipf et al. designed a selective Na^+ ion sensor by functionalizing Au-coated SiNWs with SAM.[44] The measured difference between the SAM modified and unmodified Au/SiNWs, a Na^+ sensing response of 44 mV/decade was achieved in the presence of ions including H^+, K^+, and Cl^-. Another SiNW-ISFET with the same polymer matrix as an ion-selective membrane is utilized for multi-channel analysis of inorganic ions in mixed solution and shows excellent selectivity with the interference of H^+, Na^+, and K^+.[84] Apart from ion sensing, Figure 3c demonstrated the sketch of SiNW-ISFETs for methylene blue detection. The sensors showed a near-Nernstian response of 56.4 ± 1.8 mV/decade with excellent reproducibility.

Carbon nanotubes: The carbon nanotubes (CNTs) can be lined up along the channel to act as a superhighway for electrons, which could significantly improve the electrical properties of devices. For example, when the nanotubes are well aligned in a nanochannel, the source-drain current could be much higher at the same gate voltage. Dong et al. designed a CNT-ISFET for pH-sensing, and CNTs in nanochannels are shown in Figure 3d.[85] In this work, nanochannels were generated by atomic-force microscope (AFM)-assisted nano-scratching, and the electrical properties of CNTs were tested by a current sensing AFM. Dutta et al. reported the fabrication and characterization of dual-gate CNT-ISFET for pH detection.[86] It showed a super-Nernstian sensitivity of 943 mV/pH and a suppressed drift rate down to 13.5 mV/pH. Besides, CNTs can also serve as crosslinking material for the ionophore membranes. Moreover, Cid et al. reported an ISFET based on single-walled CNTs as a transduction layer and combined with an anion-selective membrane containing valinomycin to realize the detection of K^+ down to 10^{-8} M.[87] CNTs-based ISFETs have also been reported for various biomarkers evaluation, such as acetylcholine, glucose, and laccase.[88–90]

Others: The surface potential changes due to protein binding/dissociation are usually small. As a result, current changes in ISFETs during proteins sensing are relatively difficult to identify.[91] Thus, nanostructured materials with large surface-to-volume ratios have been utilized to functionalize ISFETs for proteins sensing.[17] For instance, ISFETs based on ZnO nanorods have been demonstrated for pH testing, glucose monitoring, and DNA detection.[92–94] Recently, a novel vanadium pentoxide (V_2O_5) nanorod was also applied to construct ISFETs by Abd-Alghafour et al.

4 | GATE STRUCTURES

The modification and improvement of the ISFET's gate structure have attracted significant interest along with the development of CMOS technology. Unmodified CMOS processed ISFETs are based on the conventional FET structure with the gate metal removed and an optional sensitive membrane deposited on top of the gate. To achieve enhanced stability and sensitivity, ISFETs with dual-gates and extended gates were designed. In dual-gate ISFETs, the two gates are capacitively coupled and the dual-gate design could achieve sensitivity beyond the Nernstian limit. In extended-gate ISFETs, the sensing pads extend off the chips, and only the off-chip sensing pad is in contact with

TABLE 2 Ion-sensitive field-effect transistors (ISFETs) with different gate structures

Gate structures	Signal readout topologies	Gate materials	Applications	Pixels	Ref.
Unmodified CMOS gate	feedback mode	Si_3N_4	Detection of enterobacteria	1	[95]
Unmodified CMOS gate	Chemical-Gilbert-Cell differential mode	Poly-Si	Phage lambda DNA	32 × 32	[96]
Unmodified CMOS gate	One-differential-amplifier mode	Ta_2O_5/Poly-Si/ Si_3N_4	pH sensing	1	[52]
Dual-gate	ISFET-ISFET Differential mode	SiNW	pH sensing	1	[12]
Extended-gate	The CVCC readout	TiO_2	pH sensing	NA	[97]
Floating-gate	Current-mode	Si_3N_4/SiO_2	Real-time DNA detection	12.8K	[98]
Floating-gate	pH-to-time conversion	SiO_2	*E. coli* volume in food	512 × 576	[99]
Floating-gate	ISFET-REFET differential mode	Si_3N_4/SiO_2	DNA-based diagnostics	32 × 32	[100]
Floating-gate	The CVCC readout	Si_3N_4/SiO_2	Proton imaging	64 × 64	[101]

the solution. Moreover, ISFETs with the floating gates modulate the channel conductance with a control gate and a sensing gate. Table 2 summarizes some representative ISFETs with the as-mentioned four types of gate structures and their signal readout topologies. The corresponding mechanisms and application demonstrations will be introduced as well.

4.1 | Unmodified CMOS processed ISFETs

The fabrication of ISFETs in the unmodified CMOS process was first demonstrated by Bausells et al. in 1999.[22] Further modifications on structures were developed to enable high compatibility with the standard CMOS process, cost reduction, device scalability, and large integration density. The gate of the ISFETs in the unmodified CMOS process is extended to a passivation layer on the top, as shown in Figure 4a. The commonly used passivation layers, including Si_3N_4 and SiO_2 layers, can trap protons at the surface and enable the ISFETs to monitor pH accurately.32

Extensive applications of ISFET based on the unmodified CMOS process were reported in the following years.[58,59,102–104] Georgiou et al. proposed an ISFET-based pH sensor using a commercial 0.25-μm CMOS process.[31] A scalable CMOS-based ISFET sensing system was reported to achieve real-time DNA sequencing based on pH sensing.[58] Implementation in standard CMOS technology provides the ISFET sensing array with high sensitivity and large scalability, which further modifies the compatibility and calibration. After integration with the readout circuit and memory, a bio-sensing lab-on-chip (LoC) platform can be achieved.[105]

However, ISFETs in unmodified CMOS suffer from several drawbacks, which limit their applications. First, capacitance introduced by the passivation layer leads to extra signal attenuation. Besides, trapped charges in the passivation layer result in offset in the threshold voltage, though the as-resulted interference can be reduced using ultraviolet radiation.[106] Moreover, the change of the threshold voltage due to temperature and drift effect also limit the accuracy of the ISFET sensing.

4.2 | Dual-gate ISFETs

Diverse research aiming to increase the performance of ISFET-based sensors were reported, among which the dual-gate ISFETs were proposed to exhibit sensitivity beyond the Nernstian pH sensitivity of 59.5 mV/pH[107–109]. In dual-gate ISFETs, a bottom-gate is included in the FET and capacitive coupling between the two gates on the top and back is formed. It is known that such a dual-gate structure induces an additional charge accumulation channel, resulting in a higher current and a steeper subthreshold slope.[110] The pH sensitivity can be improved by several orders of magnitudes. Moreover, the performance limits in conventional ISFETs such as time drift and hysteresis have also been improved.[109,111]

Figure 4b shows a typical schematic of a dual-gate ISFET pH sensor.[20] The thickness of the top gate oxide and buried oxide in this device are delicately modified to enhance its immune-sensing ability. Yen et al. further studied the relations between pH sensitivity and the thickness of the sensitive layer in dual-gate ISFETs.[112] An increase in the thickness would reduce the capacitance of the sensing membrane, resulting in lower sensitivity according

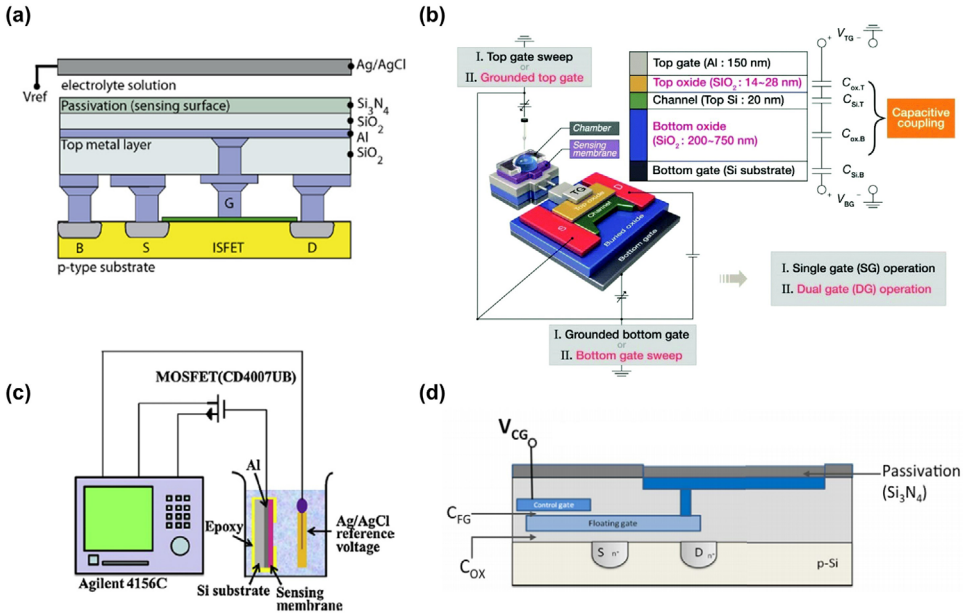

FIGURE 4 Ion-sensitive field-effect transistors (ISFETs) with different gate structures. (a) Unmodified complementary metal-oxide-semiconductor (CMOS) gate.[32] (b) Dual-gate.[20] (c) Extended-gate.[36] (d) Floating-gate[65]

to the capacitive coupling. Besides, Zhou et al. reported a dual-gate ISFET pH sensor with a high sensitivity of 720.7 mV/pH by combining SiNW.[12] An inverse dual-gate design, which leverages the SiNW as the back gate and the solution-immersed backside as the top gate, enables amplification in the threshold voltage.

4.3 | Extended-gate ISFETs

The extended-gate ISFETs are proposed to have better stability, convenient fabrication, and good reusability. Extending the gate to the top layer makes it compatible with the standard CMOS process. Moreover, the extended-gate ISFETs can be into two parts, the sensitive membrane in the solution and the FET channel region with related peripheral circuits in the dry environment. The FET circuit part can be protected well from chemical damage in such a structure, while the sensing unit can be replaced without remanufacturing the whole device.[55]

Figure 4c shows a typical extended-gate ISFET. It comprises a MoS_2 FET and aluminum-oxide/hexagonal-boron-nitride stacking sensing unit.[36] Higher pH sensitivity and low drift values are achieved. Chiu et al. proposed an extended-gate ISFET pH sensor using the tantalum doped zinc oxide (ZnO:Ta) sensitive membrane and achieved a wide linear sensing pH range.[60] Kwon et al. proposed an extended-gate ISFET pH sensor with a gate-all-around structure to achieve good sensitivity while reducing the device area.[55] However, such device structures occupy a larger area, limiting their miniaturization and integration density.

4.4 | Floating-gate ISFETs

A floating-gate ISFET consists of two gates, the sensing gate, and the control gate. The control gate provides a bias to the FET, and the sensing gate serves to convert the chemical signal from analytes to electrical signals. The control gate can provide bias in such FET, and the reference electrode can be eliminated.[64] The floating-gate ISFET was first demonstrated by Barbaro et al.[113] As shown in Figure 4d, Zhang et al. demonstrated a floating-gate ISFET for pH sensing and enzymatic reactions detection.[65] The polyaniline-functionalized sensitive membrane achieves ultrasensitive immunosensing with the 0.25-μm CMOS process.

5 | SIGNAL READOUT TOPOLOGIES

Over the past few years, the design and application of ISFET-based sensing systems have experienced dramatic evolvement. Requirements for higher accuracy and further integration improve the front-end circuit and the signal readout methods. The topologies can be classified into two types: single measurement and differential measurement.

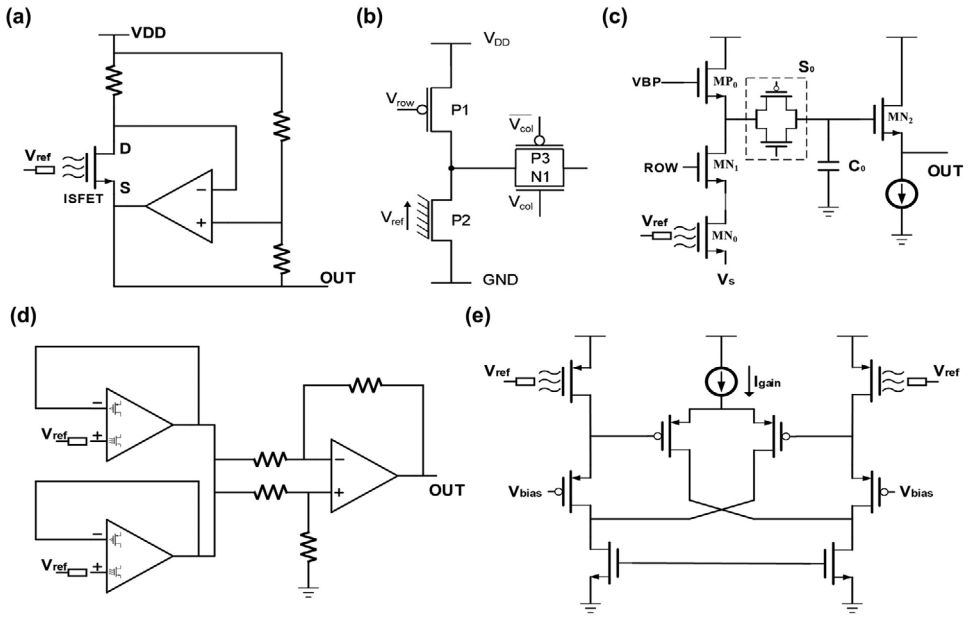

FIGURE 5 Readout topologies for ion-sensitive field-effect transistors (ISFETs). (a) Traditional source-drain follower circuit. (b) Standard pixel readout.[115] (c) pH-to-time-to-voltage readout system.[99] (d) Differential amplifier readout system.[52] (e) ISFET chemical Gilbert cell[96]

5.1 | Single measurements

In a single ISFET topology, single measurements consist of two readout methods to achieve continuous encoding. One is the feedback mode, which is the simplest readout system for the reference electrode. The ISFET's current keeps constant, and the voltage feedback to the reference varies with solution pH.[114] For instance, Kotsakis et al. addressed that the protons produced during imipenem hydrolysis could be detected using an ISFET.[95] The ISFET proved various carbapenemase-negative control strains were negative (100% specificity), which had the potential to be routinely employed in clinical laboratories for the detection of a variety of bacteria. However, due to its incompetence with the normal reference electrode, the feedback mode is replaced by the current mode. This technique is widely applied in ISFET front-end configurations, including constant-voltage, constant-current (CVCC) readout, and current-mode readout.

The CVCC readout circuit also called the source-and-drain follower, is operated at a constant drain-source voltage V_{DS} and current I_{DS}. As shown in Figure 5a, in the CVCC readout circuit, a constant voltage is loaded between the source and drain of the ISFET, and the pH variation is reflected in the changes of the source voltage V_s.[32,114] Moreover, the pixel architecture is further proposed. The readout unit for the ISFET sensor array is shown in Figure 5b, consisting of three transistors and a single ISFET device.[115] Transistor P_1 provides a constant current and serves as the load; the transmission gate P_3/N_1 connects to the column addressing line and serves as the readout for each pixel. Further combination of the pixel readout architecture with a simple source follower forms the voltage mode pixel, which is proposed by Miscourides et al.[116] The pixel circuit schematic is implemented as a source-and-drain follower where changes in V_{out} reflect the pH variation, and a total of 4096 sensor arrays occupy 0.56-mm^2 area with approximately 96 μm^2 for each pixel.

The current-mode readout is a compensation method for mismatch in large-scale ISFET arrays, which is caused by the presence of trapped charge at the sensor's floating gate. To facilitate ISFET calibration, the programmable-gate method is carried out. Miscourides et al. proposed a gradient descent algorithm by making a prior estimate of the calibration step size, thus reducing the number of iterations to one.[117] It includes standard pixel topology, chemically active pixel sensor (APS), pH-to-time conversion, and so forth. Nicholas and his coworkers introduced a large-scale ISFET for real-time DNA amplification detection. Its sensitivity was 1.03 μA/pH with 0.101 pH resolution, which was suitable for the real-time detection of carbapenemase gene *Escherichia coli* by a loop-mediated isothermal amplification.[98] Moreover, the current-mode operation in velocity-saturated devices enables their input and output characteristics (pH-current) to be perfectly linear, which is consistent with the continuous scaling trend of transistors in CMOS.

Another considerable method is pH-to-time readout, as shown in Figure 5c.[99] The capacitance C_0 is pre-charged

before detection and then discharged during the pH sensing. The discharging time is dependent on the drain-source current of the transistor MN_0, which is further related to the pH of the solution. The voltage of N_1 will relate to the pH value followed by the time-to-voltage conversion, which is achieved by turning off the switch S_0 after a certain time. Such a method enables the amplification of weak pH sensing signals. Within this topology, Liu et al. analyzed a pH-to-time readout system based on ISFET, which used a time-domain inverter as a horizontal crossover detector for a 32 × 32 array of in-pixel digital sensors. At a high frame rate of 1 kilobyte per second, the total power consumption of the system was as low as 11.286 mW.[118] In addition, a classic pH-to-time conversion was applied to demonstrate the real-time DNA amplification and detection of phage DNA loops.[58] Moser et al. demonstrated a robust ion-sensing platform with a maximum drift rate of 6.5 mV/min and an elaborate pH resolution of 0.019 pH. Furthermore, a pH-time-voltage conversion topology is proposed by Yu and co-workers to identify bacterial levels in food resources by measuring pH changes of the culture medium along with optimizing the chemical sensing area, transistor size, and discharge time.[102]

5.2 | Differential measurements

The differential measurements are also proceeded in ISFET signal readout, reducing the common-mode signal and minimizing the noise and drift.[32] Figure 5d shows the ISFET differential readout system comprising one ISFET amplifier and one differential amplifier.[52] Wong and coworkers immersed one of the ISFETs in solutions with a determined value as a reference, and the output signal indicates the difference between the two ISFET amplifiers. Then the pH of the targeted analyte can be calculated, and the drift that occurred in both ISFETs will be removed in the readout signal. It is dispensable to leverage an ideal reference electrode since differential sensing allows the elimination of any common-mode voltage between the two sensors, minimizing the effects of drift, noise attenuation, and temperature difference.[32] ISFET-ISFET differential amplifier is a common topology, which has been employed to construct a simple differential CMOS-based pH sensor by Shawkat et al.[119] The design required two different sensing areas, and the differential monolithic ISFET had a good performance in the range of 1–14 pH under the power consumption of 1.2 μW. In addition, the ISFET-reference-FET (REFET) pair in sensing arrays is another topology that draws much attention to analog front-end architecture.[114] An identical FET that is not sensitive to the measured solution is called REFET and signals can be extracted by applying a differential measurement between the paired ISFET and REFET. Cacho-Soblechero et al. designed a pixel structure with the linear operational transconductance amplifier. It converts the differential voltages V_{ISFET} and V_{DAC} into differential currents I_1 and I_2, which then generates a pulse-width modulation output signal.[100] However, different ISFET-REFET pairs could have various offsets, which limits the further improvements in sensing accuracy. Another topology named ISFET-ISFET chemical Gilbert cell was further proposed by Kalofonou et al., as shown in Figure 5e.[96] The Gilbert cell enables differential measurement of current. Low power consumption and adjustable gain can also be realized in such a design.

Looking to the future, readout circuit design plays a vital role in high-performance ISFET. For highly integrated portable and wearable sensing systems, compact size and low power consumption become more and more critical. The benefit of mature technologies in the current integrated circuit industry lies in the design and fabrication of feasible low-costing sensor circuits. Thus, the on-chip integration of sensing units, readout circuits, data storage, and transmission systems will be the future development trend.[120]

6 | BIOSENSING APPLICATIONS

ISFETs have shown great promise for the next generation of bioelectronics in clinical medicine, new drug discovery, environmental monitoring, toxic substance detection, and wearable biosensing for healthcare.[2,18,78,121,122] They have been reported for gas detection (such as CO_2, H_2, and O_2) and biosensing (such as enzyme, antibody, and antigen) in solution.[3,17,72,95,123] Compared with traditional ion-selective electrodes, ISFETs have high input impedance, low output impedance, and wideband range. They can simultaneously play the role of impedance conversion and signal amplification. As the response time of ISFET sensors is normally within several seconds, they are also capable of real-time and dynamic biosensing applications. Moreover, most of the ISFETs have high compatibility for device miniaturization and integration. Thus, they have been widely adopted for biomarkers monitoring that could indicate human body health status.

Generally, the biosensing applications of ISFETs can be categorized based on the types of biomarkers as follows: 1) Ion sensing such as H^+, Na^+, K^+, Ca^{2+}, Cl^-, and other inorganic ions. The sensitive films are generally inorganic insulation, solid or polymer films. 2) DNA sensing. It is possible to detect DNA through the protons produced due to nucleotide incorporation during a DNA amplification reaction. 3) Protein detection. The interaction of target proteins and selective membranes functionalized with

biomolecules would modulate the device surface potential, which results in measurable electric signals. 4) Microbe monitoring. ISFETs can either be directly leveraged for cellular metabolism sensing or combining the microorganism recognition layers for target analysis. Table 3 gives a summary of ISFETs for a variety of biosensing applications.

6.1 | Inorganic ions

Apart from pH sensing, ISFETs with different sensitive membranes loaded on the gates and modified channel materials realize the detection of various inorganic ions such as Na^+, K^+, Ca^{2+}, Cu^{2+}, and Cl^-. These inorganic ions serve as critical analytes in medical and healthcare applications.[8,9,125,138,139] The ion sensing mechanisms have been introduced and discussed in previous sections.

For instance, a large-area graphene-based ISFET with a detection limit of 10 nM (~39 ng/L) was achieved in real-time K^+ detection by Fakih et al.[8] As shown in Figure 6a, a layer of K^+ ionophore membrane serves as a sensing layer on a Si-SiO_2 substrate. In this ISFET, due to the charge transfer mechanism between graphene and K^+ ionophore membrane, the conductivity of graphene has changed, through which the concentration of target ions can be monitored. Potassium iodide (KI) as an important dietary supplement can also be selectively monitored by ISFETs, demonstrated by Puchnin et al.[124] By creatively adapting a self-assembled layer of calyx tubes, determination of KI was realized with a detection limit of about 30 nM. Besides, Synhaivska et al. proposed a Cu^{2+} sensitive ISFET with Si-nanoribbon and glycine–glycine–histidine (GGH) functionalized sensitive layer.[125] The interaction between the GGH and Cu^{2+} influences the net charge at the surface, thus resulting in changes in the extracted electric signals.

The development of novel sensitive materials is expected to further broaden the scope of ISFET-based ion sensing. Besides, system-level design and integration are required for practical and advanced applications.

6.2 | DNA

The combination of ISFETs and DNA detection has been successfully applied in rapid diagnosis, drug development, and agriculture engineering.[4,7] Pantelis and co-workers designed a 32 × 32 platform for DNA-based diagnostics, and the measured solution pH value was significantly reduced by 2.16 pH at room temperature due to the release of hydrogen ions during DNA amplification.[100] It is the first thermochemical ISFET array for LoC diagnostic and inspired the research advances in the field of on-chip DNA amplification and sensing.

Quantitative monitoring of DNA/RNA plays a vital role in clinical diagnostics, cancer biomarkers analysis as well as gene diagnostics/therapies. Based on ISFETs with Si_3N_4/SiO_2 sensitive layer, an LoC system was developed for breast cancer mutation point-of-care testing, which is cheaper and smaller than standard quantitative polymerase chain reaction tools.[129] As shown in Figure 6b, nucleotide incorporation during DNA amplification reaction leads to proton generation, which can be detected by the ISFETs. Multiple additions of the same nucleotide will ensure the signal is large enough to be identified and extracted. Similar to DNA sensing, ISFETs have also been used for RNA quantification. Veigas et al. proposed a platform based on ISFET for label-free quantification of RNA at room temperature.[140] Bashir and co-workers fabricated a 1024 × 1024 ISFETs array functionalized with peptide nucleic acid probe. The ISFETs array achieved reliable detection of miRNA Let-7b, which is a cancer biomarker, after hybridization of target molecules with a concentration as low as 1 nM.[130]

The combination of the ISFET array and microfluidic system also enables the detection of DNA base pairing, which is one of the most critical steps in gene sequencing. In Wu and co-workers, a biosensing array chip that contains more than 13 million sensitive units were designed to track DNA base pairs. The chip achieves a high resolution of 0.5 mV, enabling it to identify 0.01 pH changes.[141] To achieve highly accurate DNA base pairing detection, dual-mode and pH-to-time ISFET sensors could be adopted to extract adequate data from large-scale ISFETs arrays.[142]

However, the performance repeatability of DNA detection based on ISFETs is less stable. One of the main reasons is attributed to the hybridization of analytes and probes on the device surface can be largely affected by side interference. For example, it was found that ISFETs cannot reliably track the DNA hybridization process in the solution with high ionic strengths (200–300 mM). While decreasing the concentration will reduce the surface hybridization efficiency and thus inhibit signal transmission[143]. Therefore, it still requires significant research efforts in developing reliable, low-cost, and stable ISFET-based biosensors for macromolecular sensing.

6.3 | Protein

Generally, protein detection can be categorized into label and label-free analyses. For label detection, a label such as an enzyme is first attached to the target proteins. The detection of the target protein is then achieved by measuring the amount of labeled enzyme, while it is

TABLE 3 Summary of representative reports on ion-sensitive field-effect transistors (ISFETs) for biosensing applications

Biosensing application	Gate material	Gate structure	Sensitivity/ LOD	Pixel	auxiliary instrument	Novelty	Ref.
Potassium iodide (KI)	SiO_2	-	$\sim 3 \times 10^{-8}$ M	1	Microfluidic system	Higher specificity	[124]
Cu^{2+}	Al_2O_3	-	−14 mV/decade	1	Differential measurement platform	Low cost and fast response	[125]
Serum glucose and cholesterol	Si_3N_4	Floating- gate	244 ± 21 μM and 80 ± 11 μM	16×16	Colorimetric readout	Real-time test	[126]
Ethanol	SnO_2	Dual-gate	129.45 mV/decade	1	-	Higher sensitivity	[127]
Hydrazine	Cu	-	3.16 μM	1	Automated visual basic program	Low drift	[128]
Breast Cancer ESR1 Mutations	Si_3N_4/ SiO_2	Floating- gate	13 mV/pH	78×56	PCR instrument	Mutational tracking	[129]
miRNA Let-7b	HfO_2	-	1nM	1024×1024	-	Label-free	[130]
Lambda phage DNA	Si_3N_4/ SiO_2	Floating-gate	13mV/pH	78×56	Memory array	Higher SNR	[58]
Cordyceps sinensis's DNA	SiO_2/ SiNR	Dual-gate	29.3mV/pH	4	Preamplifier, Lock-in amplifier	Shorter detection time	[131]
Prostate-specific antigen	SiO_2/Si	Dual-gate	10 pM	1	Preamplifier, Lock-in amplifier	Directly clinical detection	[17]
Tetracycline repressor (bTetR)	SnO_2 NW	-	600 μg/ml	1	Microfluidic cell	Label free	[132]
C-reactive protein and immunoglobulin E	HfO_2	Dual-gate	12.5 and 125 pg/ml	128×128	-	Higher fidelity and specificity	[133]
Concanavalin A (Con A) and glucose	SiO_2	-	0.16 ng/ml and 10 nM	1	Smartphone	Long life span	[123]
Salmonella typhimurium	CeO_2	-	3 cells/ml	1	-	Low cost	[134]
E. Coli Detection	Si_3N_4	-	221 mV/pH,	4×8	Temperature sensing and optical detection	Low complexity	[135]
E. coli Screening	Si	Floating- gate	14 to 140 cfu/ml	512×576	-	High sensitivity	[136]
Influenza A virus	SiO_2	-	0–100 ng/ml	1	Microbeads and a filter-inserted bottle	One-step immunoassay	[137]

Abbreviations: polymerase chain reaction

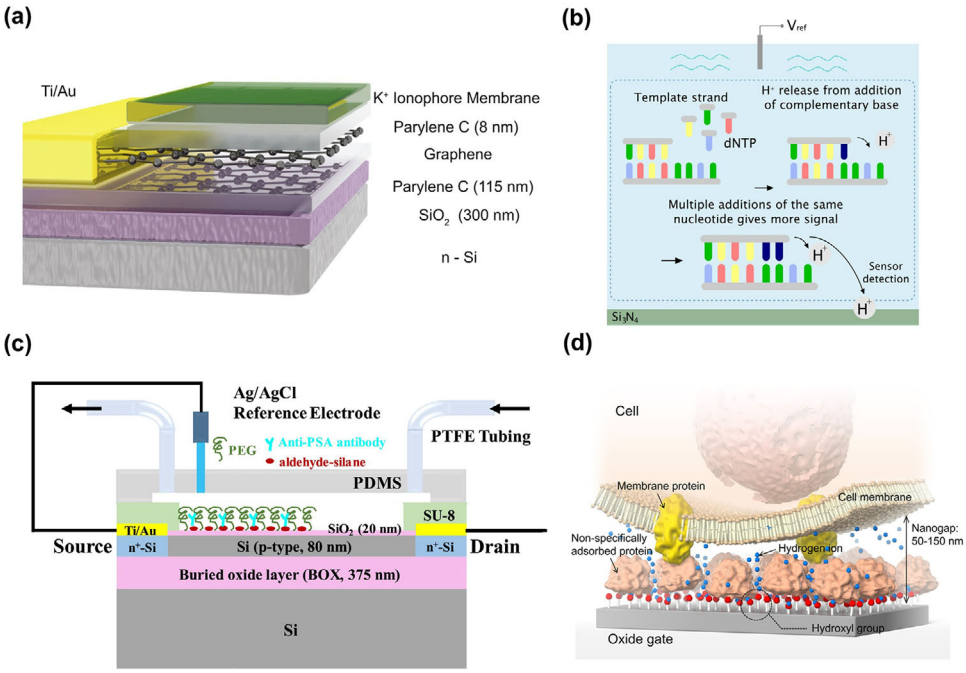

FIGURE 6 Biosensing applications of ion-sensitive field-effect transistor (ISFET) devices. (a) Schematic of a graphene-based ISFET for K^+ detection.[8] (b) Deoxyribonucleic acid (DNA) sensing based on the detection of proton generation during DNA amplification.[129] (c) Nanoribbon-based ISFET for real-time and direct detection of prostate-specific antigen.[144] (d) Schematics of cancer cell sensing at the cell/gate nanogap interface.[53]

time-consuming and normally requires expensive instruments. For label-free technologies, it can achieve real-time detection of target proteins by tracking the interaction between target proteins and receptor biomolecules. Such interaction can then be transduced into electronical, optical, or mechanical signals. Therefore, ISFETs functionalized with biomolecules be applied for label-free protein sensing.

Based on the strong bonding pair of streptavidin-biotin, Jakob et al. designed a label-free ISFET functionalized with streptavidin for the detection of tetracycline repressor biotinylated protein (bTetR).[132] The interaction of streptavidin and bTetR can modulate the electric field on the ISFET gate surface and leads to the drain-source current changes. Zhang and co-workers reported that a nanoribbon-based ISFET could detect antigens with a wider range and lower LOD.[144] As shown in Figure 6(c), the antibody immobilized on the gate layer can selectively form binding with the target antigen and the polydimethylsiloxane-based microchannel is utilized for sample delivery by polytetrafluoroethylene tubing. It was the first report on real-time and direct detection of prostate-specific antigen at concentrations from 10 pM to 1 μM in human plasma, which has high ionic strength. ISFETs for a variety of protein sensings, such as interleukin and C-reaction protein, which is highly relative to human health status, have also been successfully demonstrated recently.[145,146]

However, as the signal changes modulated by the protein's interaction are relatively weak and can be largely interfered with by background noises, their practical applications are largely limited. Device structural innovation and materials engineering on the functionalized sensitive layers are critical to further enhance the sensing sensitivity, accuracy, and reproducibility, as well as lower the fabrication costs.

6.4 | Microbes

ISFETs can be used to study microbes' metabolism, growth, and proliferation, which can be further applied in basic biomedical research as well as applications in food safety detection and tumor monitoring, and so forth. Compared with traditional techniques, such as direct plate counting, microbes sensing based on ISFETs provides a more efficient and portable option for consumer applications.

So far, ISFETs for several microorganisms have been developed, including bacteria, fungi, and viruses.[131,135,137] For instance, Yu and co-workers proposed that *E. Coli* concentration (in the range of 14–140 cfu/ml) could be screened by a 65-nm CMOS ISFET. The *E. Coli* concen-

tration can be monitored based on the pH-to-time readout circuit. The intrinsic sensitivity was improved from 33.2 to 123.8 mV/pH, more efficient screening (4 h) was achieved to differentiate the samples' *E. coli* levels (24 h).[136] In addition, other modifications for *E. coli* tests have been proposed, including reducing signal-to-noise ratio (SNR) and introducing electrophoresis.[147,148]

ISFETs for microbe sensing can also be used in the study of cellular dynamics in different growth environments. As shown in Figure 6d, Sakata et al. achieved real-time pH monitoring for the in-situ micro-environment for cancer cells. During the detection process, some proteins in the culture medium of cancer cells would adsorb on the oxidation gate. These protein macromolecules act as the insulator between the cell surface and the gate. The hydrogen ions produced by cell metabolism can easily diffuse to the gate surface and modulate the ISFET output signals. In this way, cell respiration can be monitored in real-time.[53] Tracking of other microbes such as Salmonella Typhimurium, influenza A virus has also been reported with functionalized ISFETs.[134,137]

7 | SUMMARY AND OUTLOOK

ISFETs for biosensing applications have attracted increasing research interest with the boost of biological and clinical demands. ISFET-based sensors for pH sensing are mostly in a commercialized state, while rapid advances have also been witnessed for other chemicals and bioanalytics detection, such as a variety of electrolyte ions, DNA, proteins, and microbes. In this review, we provided a general overview of ISFETs for biosensing applications, starting with an introduction to the basic mechanism of ISFET sensors. The latest advances in gate materials and gate structures that enable a large library of biomarkers detection were then illustrated. Besides, the signal readout configurations and a broad range of biosensing applications were presented.

It has been over 50 years since the invention of ISFET-based sensors, and they are expected to be integrated into smart electronic systems for broader applications. However, there are several challenges that limit the practical applications of ISFETs in biosensing. While novel analog front-end topologies have been proposed, there is a lack of standards for encoding the extracted signals.[32,96] Moreover, it usually requires specialized instruments, such as a four-probe setup or a potentiostat, to extract the measurable parameters of current, voltage, capacitance, and impedance. These instruments are either expensive or huge in volume and limit the integration of ISFETs into flexible/wearable platforms.[61149–151] In addition, the biocompatibility of the materials for ISFETs fabrication should be considered, especially for health monitoring applications as it involves contact with the human body. In general, it requires research efforts to develop and optimize the ISFET-based biosensors with reliable and reproducible sensing performance and to further integrate these ISFETs into flexible platforms so that they can either be attached to human skin conformally or be safely implanted into the human body. It is believed that ISFETs will play a significant role as an integral part of CMOS smart sensing.

ACKNOWLEDGMENTS

This work was supported by the Engineering Research Center of Integrated Circuits for Next-Generation Communications Grant (Y01796303), Southern University of Science and Technology Grant (Y01796108 and Y01796208), NSQKJJ (K21799122 and K21799109), Shenzhen Science and Technology Program Grant (KQTD20200820113051096), National Key R&D Program of the Ministry of Science and Technology Grant (2021YFE0204000) and National Natural Science Foundation of China (NSFC) Key Program Grant (62034007).

CONFLICT OF INTEREST

The authors declare that they have no conflict of interest.

REFERENCES

1. W. B. Bai, H. J. Yang, Y. J. Ma, H. Chen, J. Shin, Y. H. Liu, Q. S. Yang, I. Kandela, Z. H. Liu, S. K. Kang, C. Wei, C. R. Haney, A. Brikha, X. C. Ge, X. Feng, P. V. Braun, Y. G. Huang, W. D. Zhou, J. A. Rogers, *Adv. Mater.* **2018**, *30*, 12.
2. K. T. Upadhyay, M. K. Chattopadhyay, *Mater. Sci. Eng. B Adv. Funct. Solid-State Mater.* **2021**, *263*, 114849.
3. J. X. Zhu, X. M. Liu, Q. F. Shi, T. Y. Y. He, Z. D. Sun, X. G. Guo, W. X. Liu, O. Bin Sulaiman, B. W. Dong, C. Lee, *Micromachines* **2020**, *11*, 30.
4. L. Keeble, N. Moser, J. Rodriguez-Manzano, P. Georgiou, *IEEE Sens. J.* **2020**, *20*, 11044.
5. P. Bergveld, *IEEE Trans Biomed Eng* **1970**, *BME-17*, 70.
6. Y. C. Syu, W. E. Hsu, C. T. Lin, *ECS J. Solid State Sci. Technol.* **2018**, *7*, Q3196.
7. S. Forouhi, E. Ghafar-Zadeh, *Micromachines* **2020**, *11*, 1003.
8. I. Fakih, A. Centeno, A. Zurutuza, B. Ghaddab, M. Siaj, T. Szkopek, *Sens. Actuators B Chem.* **2019**, *291*, 89.
9. I. Fakih, O. Durnan, F. Mahvash, I. Napal, A. Centeno, A. Zurutuza, V. Yargeau, T. Szkopek, *Nat. Commun.* **2020**, *11*, 3226.
10. H. Li, Y. Zhu, M. S. Islam, M. A. Rahman, K. B. Walsh, G. Koley, *Sens. Actuators B Chem.* **2017**, *253*, 759.
11. M. Myers, F. L. M. Khir, A. Podolska, G. A. Umana-Membreno, B. Nener, M. Baker, G. Parish, *Sens. Actuators B Chem.* **2013**, *181*, 301.
12. K. Zhou, Z. D. Zhao, P. B. Yu, Z. Y. Wang, *Sens. Actuators B Chem.* **2020**, *320*, 128403.
13. J. M. Rothberg, W. Hinz, T. M. Rearick, J. Schultz, W. Mileski, M. Davey, J. H. Leamon, K. Johnson, M. J. Milgrew, M. Edwards, J. Hoon, J. F. Simons, D. Marran, J. W. Myers, J. F. Davidson, A. Branting, J. R. Nobile, B. P. Puc, D. Light, T. A. Clark, M. Huber,

J. T. Branciforte, I. B. Stoner, S. E. Cawley, M. Lyons, Y. Fu, N. Homer, M. Sedova, X. Miao, B. Reed, J. Sabina, E. Feierstein, M. Schorn, M. Alanjary, E. Dimalanta, D. Dressman, R. Kasinskas, T. Sokolsky, J. A. Fidanza, E. Namsaraev, K. J. McKernan, A. Williams, G. T. Roth, J. Bustillo, *Nature* **2011**, *475*, 348.
14. S. Nakata, T. Arie, S. Akita, K. Takei, *ACS Sens.* **2017**, *2*, 443.
15. E. Garcia-Cordero, F. Bellando, J. Zhang, F. Wildhaber, J. Longo, H. Guerin, A. M. Ionescu, *ACS Nano* **2018**, *12*, 12646.
16. A. E. Kuznetsov, N. V. Komarova, E. V. Kuznetsov, M. S. Andrianova, V. P. Grudtsov, E. N. Rybachek, K. V. Puchnin, D. V. Ryazantsev, A. N. Saurov, *Biosens. Bioelectron.* **2019**, *129*, 29.
17. S. Ma, X. Li, Y. K. Lee, A. Zhang, *Biosens. Bioelectron.* **2018**, *117*, 276.
18. K. Malpartida-Cardenas, N. Miscourides, J. Rodriguez-Manzano, L. S. Yu, N. Moser, J. Baum, P. Georgiou, *Biosens. Bioelectron.* **2019**, *145*, 111678.
19. C. Hu, I. Zeimpekis, K. Sun, S. Anderson, P. Ashburn, H. Morgan, *Anal Chem* **2016**, *88*, 4872.
20. I. K. Lee, M. Jeun, H. J. Jang, W. J. Cho, K. H. Lee, *Nanoscale* **2015**, *7*, 16789.
21. M. S. Andrianova, E. V. Kuznetsov, V. P. Grudtsov, A. E. Kuznetsov, *Biosens. Bioelectron.* **2018**, *119*, 48.
22. J. Bausells, J. Carrabina, A. Errachid, A. Merlos, *Sens. Actuators B Chem.* **1999**, *57*, 56.
23. P. Salvo, B. Melai, N. Calisi, C. Paoletti, F. Bellagambi, A. Kirchhain, M. G. Trivella, R. Fuoco, F. Di Francesco, *Sens. Actuators B Chem.* **2018**, *256*, 976.
24. H. Wang, P. Zhao, X. Zeng, C. D. Young, W. Hu, *Nanotechnology* **2019**, *30*, 375203.
25. A. S. Poghossian, *Sens. Actuators B Chem.* **1992**, *7*, 367.
26. A. Das, D. H. Ko, C. -H. Chen, L. -B. Chang, C. -S. Lai, F. -C. Chu, L. Chow, R. -M. Lin, *Sens. Actuators B Chem.* **2014**, *205*, 199.
27. D. E. Yates, S. Levine, T. W. Healy, *J. Chem. Soc., Faraday Trans. 1* **1974**, *70*, 1807.
28. G. A. Bootsma, N. F. De Rooij, A. van Silfhout, *Sens. Actuator* **1981**, *1*, 111.
29. L. Bousse, N. F. De Rooij, P. Bergveld, *IEEE Trans. Electron Devices* **1983**, *30*, 1263.
30. A. Vandenberg, P. Bergveld, D. N. Reinhoudt, E. J. R. Sudholter, *Sens. Actuator* **1985**, *8*, 129.
31. P. Georgiou, C. Toumazou, *Sens. Actuators B Chem.* **2009**, *143*, 211.
32. N. Moser, T. S. Lande, C. Toumazou, P. Georgiou, *IEEE Sens. J.* **2016**, *16*, 6496.
33. A. P. P. Alves, L. M. Meireles, G. A. Ferrari, T. H. R. Cunha, M. O. Paraense, L. C. Campos, R. G. Lacerda, *Appl. Phys. Lett.* **2020**, *117*, 033105.
34. S. H. Jung, Y. M. Seo, T. Gu, W. Jang, S. G. Kang, Y. Hyeon, S. H. Hyun, J. H. Lee, D. Whang, *Nano Lett.* **2021**, *21*, 34.
35. Y.-H. Chang, Y.-S. Lu, Y.-L. Hong, S. Gwo, J. A. Yeh, *IEEE Sens. J* **2011**, *11*, 1157.
36. W. Wei, Z. Zeng, W. Liao, W. K. Chim, C. Zhu, *ACS Appl. Nano Mater.* **2019**, *3*, 403.
37. J. J. Shan, J. H. Li, X. Y. Chu, M. Z. Xu, F. J. Jin, X. J. Wang, L. Ma, X. Fang, Z. P. Wei, X. H. Wang, *Rsc Adv.* **2018**, *8*, 7942.
38. G. H. Zhou, J. B. Chang, H. H. Pu, K. Y. Shi, S. Mao, X. Y. Sui, R. Ren, S. M. Cui, J. H. Chen, *ACS Sens.* **2016**, *1*, 295.
39. Y. Chen, R. Ren, H. Pu, J. Chang, S. Mao, J. Chen, *Biosens. Bioelectron.* **2017**, *89*, 505.
40. G. H. Zhou, H. H. Pu, J. B. Chang, X. Y. Sui, S. Mao, J. H. Chen, *Sens. Actuators B Chem.* **2018**, *257*, 214.
41. Y. Li, Z. Peng, N. J. Holl, M. R. Hassan, J. M. Pappas, C. Wei, O. H. Izadi, Y. Wang, X. Dong, C. Wang, Y.-W. Huang, D. Kim, C. Wu, *ACS Omega* **2021**, *6*, 6643.
42. C. B. Liu, X. J. Wei, S. B. Hao, B. Y. Zong, X. Y. Chen, Z. Li, S. Mao, *Anal. Chem.* **2021**, *93*, 8010.
43. O. Knopfmacher, A. Tarasov, W. Fu, M. Wipf, B. Niesen, M. Calame, C. Schonenberger, *Nano Lett* **2010**, *10*, 2268.
44. M. Wipf, R. L. Stoop, A. Tarasov, K. Bedner, W. Fu, I. A. Wright, C. J. Martin, E. C. Constable, M. Calame, C. Schonenberger, *ACS Nano* **2013**, *7*, 5978.
45. M. Kaisti, *Biosens. Bioelectron.* **2017**, *98*, 437.
46. P. Bergveld, *IEEE Trans. Biomed. Eng.* **1972**, *BME-19*, 342.
47. S. Honda, M. Shiomi, T. Yamaguchi, Y. Fujita, T. Arie, S. Akita, K. Takei, *Advanced Electronic Materials* **2020**, *6*, 2000583.
48. J. Zhang, M. Rupakula, F. Bellando, E. Garcia Cordero, J. Longo, F. Wildhaber, G. Herment, H. Guerin, A. M. Ionescu, *ACS Sens.* **2019**, *4*, 2039.
49. W. Xiao, N. Miscourides, P. Georgiou, in *IEEE Int. Symp. Circuits Syst.*, IEEE, Baltimore, MD, **2017**, 1.
50. H. -J. Jang, W. -J. Cho, *Appl. Phys. Lett.* **2011**, *99*, 043703.
51. T. Matsuo, M. Esashi, *Sens. Actuator* **1981**, *1*, 77.
52. H. S. Wong, M. H. White, *IEEE Trans. Electron Devices* **1989**, *36*, 479.
53. T. Sakata, H. Sugimoto, A. Saito, *Anal Chem* **2018**, *90*, 12731.
54. H. Abe, M. Esashi, T. Matsuo, *IEEE Trans. Electron Devices* **1979**, *26*, 1939.
55. J. Kwon, B. H. Lee, S. Y. Kim, J. Y. Park, H. Bae, Y. K. Choi, J. H. Ahn, *ACS Sens.* **2019**, *4*, 1724.
56. P. Firek, M. Waskiewicz, B. Stonio, J. Szmidt, *Mater. Sci.* **2015**, *33*, 669.
57. R. Chaudhary, A. Sharma, S. Sinha, J. Yadav, R. Sharma, R. Mukhiya, V. K. Khanna, *IET Comput. Digit. Tech.* **2016**, *10*, 268.
58. N. Moser, J. Rodriguez-Manzano, T. S. Lande, P. Georgiou, *IEEE Trans. Biomed. Circuits Syst.* **2018**, *12*, 390.
59. C. Toumazou, L. M. Shepherd, S. C. Reed, G. I. Chen, A. Patel, D. M. Garner, C. J. Wang, C. P. Ou, K. Amin-Desai, P. Athanasiou, H. Bai, I. M. Brizido, B. Caldwell, D. Coomber-Alford, P. Georgiou, K. S. Jordan, J. C. Joyce, M. La Mura, D. Morley, S. Sathyavruthan, S. Temelso, R. E. Thomas, L. Zhang, *Nat. Methods* **2013**, *10*, 641.
60. Y. -S. Chiu, C.-T. Lee, L. -R. Lou, S. -C. Ho, C. -T. Chuang, *Sens. Actuators B Chem.* **2013**, *188*, 944.
61. J. H. Jeon, W. J. Cho, *Sci. Technol. Adv. Mater.* **2020**, *21*, 371.
62. C. -H. Lu, T. -H. Hou, T. -M. Pan, *IEEE Trans. Electron Devices* **2018**, *65*, 237.
63. K. Singh, J. -L. Her, B. -S. Lou, S. -T. Pang, T. -M. Pan, *IEEE Electron Device Lett.* **2019**, *40*, 804.
64. Z. Qi, H. S. Majumdar, M. Kaisti, A. Prabhu, A. Ivaska, R. Osterbacka, A. Rahman, K. Levon, *IEEE Trans. Electron Devices* **2015**, *62*, 1291.
65. Q. Zhang, M. Kaisti, A. Prabhu, Y. Yu, Y.-A. Song, M. H. Rafailovich, A. Rahman, K. Levon, *Electrochim. Acta* **2018**, *261*, 256.
66. T. Kajisa, T. Sakata, *Sci. Technol. Adv. Mater.* **2017**, *18*, 26.

67. M. Hosseini, M. Fathollahzadeh, M. Kolahdouz, A. Rostamian, M. Mahmoodian, A. Samaeian, H. H. Radamson, *J. Solid State Electrochem.* **2018**, *22*, 3161.
68. R. Jarmin, K. Y. Lee, H. Hashim, N. Denis, N. A. Rashid, M. A. M. Noor, *IEEE International Conference on Biomedical Engineering and Sciences*, Miri, Malaysia, **2014**, pp. 561.
69. L. F. Chen, H. Yu, J. S. Zhong, J. Wu, W. T. Su, *J. Alloy Compd.* **2018**, *749*, 60.
70. B. Nasri, T. Wu, A. Alharbi, M. Gupta, R. RanjitKumar, S. Sebastian, Y. Wang, R. Kiani, D. Shahrjerdi, *ISSCC Dig. Tech. Pap. I* **2017**, 268.
71. J. Chang, H. Pu, S. A. Wells, K. Shi, X. Guo, G. Zhou, X. Sui, R. Ren, S. Mao, Y. Chen, M. C. Hersam, J. Chen, *Mol. Syst. Design Eng.* **2019**, *4*, 491.
72. S. Kim, G. Lee, J. Kim, *ECS J. Solid State Sci. Technol.* **2018**, *7*, Q3065.
73. B. Radisavljevic, A. Radenovic, J. Brivio, V. Giacometti, A. Kis, *Nat. Nanotechnol.* **2011**, *6*, 147.
74. H. L. Wang, P. Zhao, X. Zeng, C. D. Young, W. Hu, *Nanotechnology* **2019**, *30*, 375203.
75. C. Zheng, X. Jin, Y. T. Li, J. C. Mei, Y. J. Sun, M. M. Xiao, H. Zhang, Z. Y. Zhang, G. J. Zhang, *Sci. Rep.* **2019**, *9*, 759.
76. Y. J. Yang, B. Zeng, Y. X. Li, H. G. Liang, Y. B. Yang, Q. Yuan, *Sci. Chin. -Chem.* **2020**, *63*, 997.
77. X. Li, Y. L. Lu, Q. J. Liu, *Talanta* **2021**, *235*, 122726.
78. S. B. Hao, C. B. Liu, X. Y. Chen, B. Y. Zong, X. J. Wei, Q. J. Li, H. H. Qin, S. Mao, *J. Hazard. Mater.* **2021**, *418*, 126301.
79. C. B. Liu, S. B. Hao, X. Y. Chen, B. Y. Zong, S. Mao, *ACS Appl. Mater. Interfaces* **2020**, *12*, 32970.
80. B. Z. Xu, M. S. Zhu, W. C. Zhang, X. Zhen, Z. X. Pei, Q. Xue, C. Y. Zhi, P. Shi, *Adv. Mater.* **2016**, *28*, 3333.
81. S. Kim, T. Rim, K. Kim, U. Lee, E. Baek, H. Lee, C. K. Baek, M. Meyyappan, M. J. Deen, J. S. Lee, *Analyst* **2011**, *136*, 5012.
82. E. Buitrago, M. F.-B. Badia, Y. M. Georgiev, R. Yu, O. Lotty, J. D. Holmes, A. M. Nightingale, H. M. Guerin, A. M. Ionescu, *Sens. Actuators B Chem.* **2014**, *199*, 291.
83. S.-K. Cho, W.-J. Cho, *Sens. Actuators B Chem.* **2021**, *326*, 128835.
84. X. Chen, Q. Hu, S. Chen, N. L. Netzer, Z. Wang, S.-L. Zhang, Z. Zhang, *Sens. Actuators B Chem.* **2018**, *270*, 89.
85. Z. Dong, U. C. Wejinya, S. N. S. Chalamalasetty, *Sens. Actuators B Phys.* **2012**, *173*, 293.
86. J. C. Dutta, H. R. Thakur, G. Keshwani, *IEEE Sens. J.* **2019**, *19*, 5692.
87. C. C. Cid, J. Riu, A. Maroto, F. X. Rius, *Analyst* **2008**, *133*, 1001.
88. P. K. Sharma, H. R. Thakur, J. C. Dutta, *J. Comp. Electron.* **2017**, *16*, 584.
89. D. Lee, T. Cui, *Biosens. Bioelectron.* **2010**, *25*, 2259.
90. S. Ebrahimi, Z. E. Nataj, S. Khodaverdian, A. Khamsavi, Y. Abdi, K. Khajeh, *IEEE Sens. J.* **2020**, *20*, 14590.
91. I. Zeimpekis, K. Sun, C. Hu, N. M. J. Ditshego, O. Thomas, M. R. R. de Planque, H. M. H. Chong, H. Morgan, P. Ashburn, *Nanotechnology* **2016**, *27*, 165502.
92. S. J. Young, L. T. Lai, W. L. Tang, *IEEE Sens. J.* **2019**, *19*, 10972.
93. M. Hajmirzaheydarali, M. Akbari, A. Shahsafi, S. Soleimani-Amiri, M. Sadeghipari, S. Mohajerzadeh, A. Samaeian, M. A. Malboobi, *IEEE Electron Device Lett.* **2016**, *37*, 663.
94. C. T. Lee, Y. S. Chiu, *Sens. Actuators B Chem.* **2015**, *210*, 756.
95. S. D. Kotsakis, G. Miliotis, E. Tzelepi, L. S. Tzouvelekis, V. Miriagou, *Sci. Rep.* **2021**, *11*, 12061.
96. M. Kalofonou, C. Toumazou, *IEEE Trans. Biomed. Circuits Syst.* **2014**, *8*, 565.
97. H. Guliga, W. F. H. Abdullah, S. H. Herman, in *2nd Int. Conf. Electr. Electron. Syst. Eng.*, Kuala Lumpur, MALAYSIA, **2015**, pp. 11.
98. N. Miscourides, L. S. Yu, J. Rodriguez-Manzano, P. Georgiou, *IEEE Trans. Biomed. Circuits Syst.* **2018**, *12*, 1202.
99. Y. Jiang, X. Liu, T. C. Dang, M. Yan, H. Yu, J. C. Huang, C. H. Hsieh, T. T. Chen, in *36th IEEE Symp. VLSI Technol.*, Honolulu, HI, **2016**, pp. 1.
100. M. Cacho-Soblechero, K. Malpartida-Cardenas, C. Cicatiello, J. Rodriguez-Manzano, P. Georgiou, *IEEE Trans. Biomed. Circuits Syst.* **2020**, *14*, 477.
101. B. Nemeth, M. S. Piechocinski, D. R. S. Cumming, *Sens. Actuators B Chem.* **2012**, *171-172*, 747.
102. Y. Jiang, X. Liu, T. C. Dang, X. Huang, H. Feng, Q. Zhang, H. Yu, *IEEE Trans. Biomed. Circuits Syst.* **2018**, *12*, 402.
103. Y. Q. Hu, P. Georgiou, in: *2018 IEEE Biomed. Circuits Syst. Conf.* IEEE, **2018**, 69.
104. Y. Hu, N. Moser, P. Georgiou, *IEEE Sens. J.* **2017**, *17*, 5276.
105. N. Moser, L. Keeble, J. Rodriguez-Manzano, P. Georgiou, *2019 26th IEEE Int. Conf. Electron. Circuits Syst*. Geneva, Italy, **2019**, 57.
106. P. Hammond, *Microelectron. Eng.* **2004**, *73-74*, 893.
107. J. Go, P. R. Nair, M. A. Alam, *J. Appl. Phys.* **2012**, *112*, 034516.
108. H. -J. Jang, W. -J. Cho, *Appl. Phys. Lett.* **2012**, *100*, 073701.
109. J. -K. Park, H. -J. Jang, J. -T. Park, W. -J. Cho, *Solid-State Electron.* **2014**, *97*, 2.
110. G. H. Gelinck, E. van Veenendaal, R. Coehoorn, *Appl. Phys. Lett.* **2005**, *87*, 073508.
111. Y. J. Huang, C. C. Lin, J. C. Huang, C. H. Hsieh, C. H. Wen, T. T. Chen, L. S. Jeng, C. K. Yang, J. H. Yang, F. Tsui, Y. S. Liu, S. Liu, M. Chen, *2015 IEEE Int. Electron. Devices Meet*. Washington, DC, **2015**.
112. L. -C. Yen, M. -T. Tang, C. -Y. Tan, T. -M. Pan, T. -S. Chao, *IEEE Electron Device Lett.* **2014**, *35*, 1302.
113. M. Barbaro, A. Bonfiglio, L. Raffo, *IEEE Trans. Electron Devices* **2006**, *53*, 158.
114. P. Bergveld, *Sens. Actuators B Chem.* **2003**, *88*, 1.
115. B. Nemeth, M. S. Piechocinski, D. R. S. Cumming, *Sens. Actuators B Chem.* **2012**, *171-172*, 747.
116. N. Miscourides, P. Georgiou, *IEEE Sens. J.* **2019**, *19*, 1224.
117. N. Miscourides, P. Georgiou, in *2019 IEEE Int. Symposium on Circuits and Systems*, IEEE, Sapporo, Japan, **2019**, pp. 1.
118. Y. Liu, T. G. Constandinou, P. Georgiou, *IEEE Trans. Biomed. Circuits Syst.*, **2019**, *13*, 1201.
119. M. S. A. Shawkat, N. McFarlane, *IEEE Sens.*, **2017**, 148.
120. N. T. Thet, J. Mercer-Chalmers, R. J. Greenwood, A. E. R. Young, K. Coy, S. Booth, A. Sack, A. T. A. Jenkins, *ACS Sens.* **2020**, *5*, 2652.
121. H. Y. Nyein, W. Gao, Z. Shahpar, S. Emaminejad, S. Challa, K. Chen, H. M. Fahad, L. C. Tai, H. Ota, R. W. Davis, A. Javey, *ACS Nano* **2016**, *10*, 7216.
122. X. Zeng, R. Peng, Z. Fan, Y. Lin, *Mater. Today Energy* **2022**, *23*, 100900.
123. S. Zhao, C. Shi, H. Y. Hu, Z. P. Li, G. Xiao, Q. C. Yang, P. Sun, L. Y. Cheng, W. C. Niu, J. S. Bi, Z. Yue, *Biosens. Bioelectron.* **2020**, *151*, 111962.

124. K. Puchnin, M. Andrianova, A. Kuznetsov, V. Kovalev, *Biosens. Bioelectron.* **2017**, *98*, 140.
125. O. Synhaivska, Y. Mermoud, M. Baghernejad, I. Alshanski, M. Hurevich, S. Yitzchaik, M. Wipf, M. Calame, *Sensors* **2019**, *19*, 4022.
126. C. X. Hu, M. A. Al-Rawhani, B. C. Cheah, S. Velugotla, D. R. S. Cumming, *IEEE Sens. J.* **2018**, *18*, 484.
127. C. M. Lim, J. Y. Kwon, W. J. Cho, *ACS Appl. Mater. Interfaces* **2017**, *9*, 14051.
128. A. Farhangfar, *IEEE Sens. J.* **2018**, *18*, 925.
129. G. Alexandrou, N. Moser, K. T. Mantikas, J. Rodriguez-Manzano, S. Ali, R. C. Coombes, J. Shaw, P. Georgiou, C. Toumazou, M. Kalofonou, *IEEE Trans. Biomed. Circuits Syst.* **2021**, *15*, 380.
130. A. Ganguli, Y. Watanabe, M. T. Hwang, J. C. Huan, R. Bashir, *Biomed. Microdevices* **2018**, *20*, 45.
131. S. H. Ma, Y. K. Lee, A. P. Zhang, X. Li, *Sensor Actuat B-Chem* **2018**, *264*, 344.
132. M. H. Jakob, B. Dong, S. Gutsch, C. Chatelle, A. Krishnaraja, W. Weber, M. Zacharias, *Nanotechnology* **2017**, *28*, 245503.
133. D. S. Juang, C. H. Lin, Y. R. Huo, C. Y. Tang, C. R. Cheng, H. S. Wu, S. F. Huang, A. Kalnitsky, C. C. Lin, *Biosens. Bioelectron.* **2018**, *117*, 175.
134. N. F. Starodub, J. O. Ogorodnijchuk, *Electroanalysis* **2012**, *24*, 600.
135. M. Z. Duan, X. P. Zhong, X. Zhao, O. M. El-Agnaf, Y. K. Lee, A. Bermak, *IEEE Trans. Biomed. Circuits Syst.* **2021**, *15*, 497.
136. Y. Jiang, X. Liu, T. C. Dang, X. W. Huang, H. Feng, Q. Zhang, H. Yu, *IEEE Trans. Biomed. Circuits Syst.* **2018**, *12*, 402.
137. J. H. Bong, H. R. Kim, J. W. Yoo, M. J. Kang, M. G. Shin, J. S. Lee, W. B. Shim, S. D. Lee, J. C. Pyun, *Biosens. Bioelectron.* **2020**, *165*, 112341.
138. N. Jaffrezicrenault, J. M. Chovelon, H. Perrot, P. Leperchec, Y. Chevalier, *Sens. Actuators B Chem.* **1991**, *5*, 67.
139. X. X. Yuan, X. L. Zhang, Y. Z. Huang, J. Y. Jie, Q. Q. Wei, M. Q. Tan, Y. D. Yu, *Int J Electrochem Sci* **2021**, *16*, 150911.
140. B. Veigas, J. Pinto, R. Vinhas, T. Calmeiro, R. Martins, E. Fortunato, P. V. Baptista, *Biosens. Bioelectron.* **2017**, *91*, 788.
141. P. Sun, Y. X. Cong, M. Xu, H. Q. Si, D. Zhao, D. P. Wu, *Micromachines* **2021**, *12*, 731.
142. S. M. Peter, M. K. James, P. B. Dhanusha, H. Mathew, in *Int. Conf. Intell. Comp. Instrument. Control Technol.*, Kannur, INDIA, **2017**, pp. 307.
143. X. Xu, A. Makaraviciute, E. Abdurakhmanov, F. Wermeling, S. Li, U. H. Danielson, L. Nyholm, Z. Zhang, *ACS Sensors* **2020**, *5*, 217
144. S. H. Ma, X. Li, Y. K. Lee, A. P. Zhang, *Biosens. Bioelectron.* **2018**, *117*, 276.
145. D. Rani, Y. Singh, M. Salker, X. T. Vu, S. Ingebrandt, V. Pachauri, *Anal. Bioanal. Chem.* **2020**, *412*, 6777.
146. O. Kutova, M. Dusheiko, N. I. Klyui, V. A. Skryshevsky, *Microelectron. Eng.* **2019**, *215*, 110993.
147. M. Castellarnau, N. Zine, J. Bausells, C. Madrid, A. Juarez, J. Samitier, A. Errachid, *Sens. Actuators B Chem.* **2007**, *120*, 615.
148. M. Z. Duan, X. P. Zhong, J. T. Xu, Y. K. Lee, A. Bermak, *IEEE Trans. Biomed. Circuits Syst.* **2020**, *14*, 463.
149. S. Nakata, M. Shiomi, Y. Fujita, T. Arie, S. Akita, K. Takei, *Nat. Electron.* **2018**, *1*, 596.
150. Q. F. Li, J. Q. Zhao, Y. K. Huang, W. Tang, S. Peng, S. Qiu, Q. Q. Zhang, X. J. Guo, *IEEE Electron Device Letters* **2018**, *39*, 591.
151. X. Ma, Z. Jiang, Y. Lin, *J. Semicond.* **2021**, *42*, 101602.

AUTHOR BIOGRAPHIES

Xiaohao Ma received his B.E. degree from the Southern University of Science and Technology in 2018. He is currently a Ph.D. student in the joint program of Southern University of Science and Technology and Hong Kong Polytechnic University. His research focuses on textile-based sensors.

Ruiheng Peng got his B.E. degree from the Southern University of Science and Technology in 2020. He is currently an MS student at the University of Southern California, focusing on computer architecture and VLSI design.

Dr. Wei Mao received the B.Eng. and Ph.D. degree in electrical engineering from Southeast University in 2011 and the National University of Singapore (NUS) in 2017, respectively. Since Dec. 2019, he has been with the Southern University of Science and Technology (SUSTech) as a Research Assistant Professor. His research interests include mixed-signal integrated circuits and AI hardware accelerators.

Yuanjing Lin received her Ph.D. degree in Electronic and Computer Science, Hong Kong University of Science and Technology in 2018. From 2019 to 2020, she was a Postdoctoral Fellow in Electrical Engineering and Computer Sciences at the University of California, Berkeley. She is currently an Assistant Professor at the Southern University of Science and Technology. Her research interests focus on flexible electronics and wearable sensing systems.

Dr. Hao Yu received the Ph.D. degree in electrical engineering from the Department of Electrical Engineering, University of California, Los Angeles, USA, in 2007. He is currently with the Southern University of Science and Technology as a Professor. He is a senior member of IEEE and ACM. His research interests include energy-efficient data links, sensors, and analysis.

How to cite this article: X. Ma, R. Peng, W. Mao, Y. Lin, H. Yu, *Electrochem. Sci. Adv.* **2022**, e2100163. https://doi.org/10.1002/elsa.202100163